CHEMISTRY
A European Journal

A Journal of
ChemPubSoc Europe

Accepted Article

Title: Readily Accessible and Predictable Naphthalene-based Two-photon Fluorophore with Full Visible-color Coverage

Authors: Ja Young Koo; Cheol Ho Heo; Young-Hee Shin; Dahahm Kim; Chang Su Lim; Bong Rae Cho; Hwan Myung Kim; Seung Bum Park

To be cited as: Chem. Eur. J. 10.1002/chem.201603496

Link to VoR: http://dx.doi.org/10.1002/chem.201603496

Supported by
ACES

WILEY-VCH

10.1002/chem.201603496

WILEY-VCH

Readily Accessible and Predictable Naphthalene-based Two-photon Fluorophore with Full Visible-color Coverage

Ja Young Koo,[a] Cheol Ho Heo,[b] Young-Hee Shin,[a] Dahahm Kim,[a] Chang Su Lim,[b] Bong Rae Cho,[c] Hwan Myung Kim,[b] and Seung Bum Park*[a,d]

This manuscript is dedicated to 60th birthday of Prof. Stuart L. Schreiber.

Abstract: Herein we reported 22 acedan-derived two-photon fluorophores with synthetic feasibility and a full coverage of visible color emission. Their emission wavelengths were well predicted by in silico analysis, which enabled us to visualize multicolor images by two-photon excitation with single wavelength, and to design a turn-on two-photon fluorescence sensor for endogenous H_2O_2 in Raw 264.7 macrophage and rat brain hippocampus ex vivo.

To explore the deep inside of biological systems, fluorescent organic molecules have been essential and powerful materials as a visualization tool due to their ease of handling, low cost, high sensitivity, and bypassing radioactive materials.[1] As bioimaging technologies have been developed, two-photon microscopy has emerged in a last few decades to overcome the limitation of one-photon fluorescence microscopy. By virtue of near-IR light excitation, two-photon organic fluorophores have their own advantages for bioimaging such as the increased penetration depth for *ex vivo* imaging, tolerance toward photo-damages and photo-bleaching, and localized excitation.[2]

Among two-photon organic fluorophores, acedan (**1a**)—naphthalene-based fluorophore containing dipolar donor-bridge-acceptor system (D-π-A)[3,4]—has been the most popular structural motif for the biological applications and has been utilized in monitoring various biological events such as changes in metal ions,[5] pH,[6] reactive oxygen species,[7] and other metabolites.[8] Due to the fact that acedan emits bright fluorescence by single-photon excitation as well as two-photon excitation despite its relatively simple structure, its analogues have been developed for two-photon bioimaging.

However, structure-photophysical property relationship (SPPR) studies of acedan-derived fluorophores have not yet been pursued systematically. This SPPR information is important for designing bioprobes to visualize biological systems with multicolor windows and helpful to select appropriate two-photon fluorophores with desired photophysical properties for certain biological applications. Along with expanding our knowledge of two-photon fluorophores derived from naphthalene-based D-π-A system, we focused on a rational approach for designing bright two-photon fluorophores with synthetic feasibility as well as a full visible-color coverage of emission wavelength (λ_{em}).

Looking in-depth, acedan **1a** is composed of simple naphthalene core skeleton with two substituents, 2-acetyl and 6-dimethylamino groups with opposite electronic characters, at the opposite directions. The photophysical property of this common structural motif can be explained by intramolecular charge transfer (ICT)[9] process; electronic perturbation through π-electron linkage from electron-donating part (6-dimethylamino group) to electron-withdrawing part (2-acetyl group) is observed at the calculated excited states of **1a**, which makes it a typical example of organic fluorophores containing the dipolar D-π-A system (Figure 1a). As **1a** emits fluorescence at blue-to-green

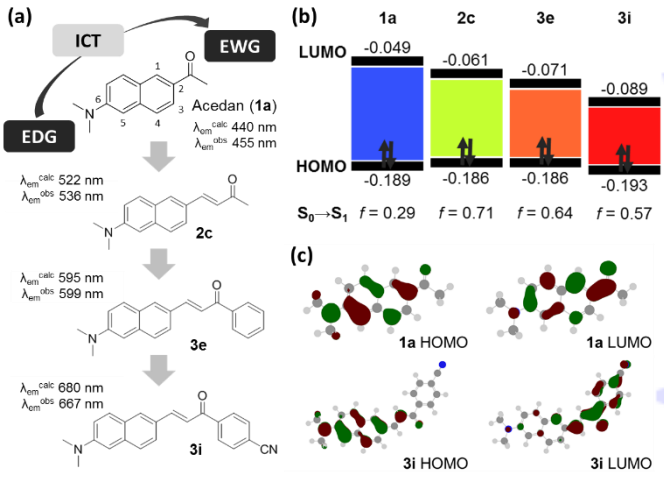

Figure 1. Design principle of naphthalene-based fluorophores from **1a** to **2c**, **3e**, and **3i**. a) Designing streamline of naphthalene-based fluorophores from blue to red fluorescence. λ_{em}^{calc} : Predicted emission wavelength (nm) (see Table S1); λ_{em}^{obs} : Observed emission wavelength (nm). b) HOMO and LUMO energy levels and energy gaps of representative fluorophores (**1a**, **2c**, **3e**, and **3i**). c) Molecular orbital lobes of **1a** and **3i** at HOMO and LUMO states. Larger shift of orbital lobes was observed in **3i** than **1a**.

colored region (455 nm in DMF and 515 nm in water[4]), we aimed its structural modification for bathochromic shift of emission wavelength. Before the actual synthesis of

[a] J. Y. Koo, Dr. Y.-H. Shin, D. Kim, and Prof. Dr. S. B. Park.
Department of Chemistry, Seoul National University
Seoul 08826 (Korea)
Fax: (+82)2-884-4025, E-mail: sbpark@snu.ac.kr

[b] C. H. Heo, Dr. C. S. Lim, and Prof. Dr. H. M. Kim.
Department of Chemistry, Division of Energy System Research
Ajou University, Suwon 16499 (Korea)

[c] Prof. Dr. B. R. Cho
Department of Chemistry, Daejin University, Pochun 11159
(Korea)

[d] Prof. Dr. S. B. Park.
Department of Biophysics and Chemical Biology
Seoul National University, Seoul 08826 (Korea)

Supporting information for this article is given via a link at the end of the document.

fluorophores derived from **1a**, we carried out *in silico* analysis to obtain the structural insight for the rational modification of **1a** to mimimize trials and errors. In fact, our previous studies clearly demonstrated that the emission wavelength of organic fluorophores are inversely correlated to the energy gap between the highest occupied molecular orbital (HOMO) and the lowest unoccupied molecular orbital (LUMO).[10,11] Their molar absorptivity (ε) is also positively correlated with S_0–S_1 oscillator strength.[11,12] Based on this guideline, we designed a series of analogues of **1a** with a decrease of HOMO–LUMO energy gap to achieve red-shifted emission wavelengths.

When we introduced various substituents, instead of dimethylamino group, at the C-6 position of **1a**, we observed wider HOMO–LUMO energy gaps (Figure S1). In contrast, the introduction of additional π-conjugation system, various functional groups, and substituted aryl/heteroaryl groups at the C-2 position of **1a** led to narrower HOMO–LUMO energy gaps. As shown in Figure 1a, a simple insertion of olefin unit between naphthyl and carbonyl group resulted in **2c** with 82-nm red shift in the predicted emission wavelength. The further extension of π-conjugation system via additional phenyl ring beside carbonyl group in **2c** generated **3e**, which was predicted to have an additional 73-nm red shift. 4-cyanophenyl-containing **3i** predicted to show additional 85-nm bathochromic shift from **3e**. Interestingly, **3i** was predicted to have 212 nm red-shifted emission wavelength compared to that of **1a**. The increase of electron-withdrawing natures at the C-2 position of **1a** via an extension of π-conjugation system or an introducing more electron-withdrawing substituents lowers the LUMO energy (Figure 1b). Due to the fact that the lowering of LUMO energy strongly influences the ICT process of dipolar D-π-A system, these rational modifications of **1a** caused larger shifts of orbital lobes between HOMO and LUMO (Figure 1c).

For the practical usage of organic fluorophores, it is essential to have a readily accessible synthetic route. In our naphthalene-based two-photon fluorophores, all desired compounds were prepared within one- or two-step synthesis from previous reported intermediate **5**. As shown in Scheme 1, Pd-mediated Heck-type coupling reaction of **5** with various α,β-unsaturated carbonyl compounds yielded the desired fluorophores in a single step (General Procedure **A**). The identical set of organic fluorophores can be achieved using aldehyde-containing **1b** obtained by lithiation of **5** with n-BuLi and the subsequent formylation via the substitution with DMF.[13] The resulting intermediate **1b** was transformed to the desired fluorophores via simple aldol condensation (General Procedure **B**). Using this synthetic strategy, we prepared four classes of naphthalene-based two-photon fluorophores. Class I consists of original acedan (**1a**) and formyl-substituted analogue **1b**. Two-photon organic fluorophores in Class II, III, and IV were prepared by either General Procedure A or B. Class II contains olefin-inserted acedan (**2c**) and their analogues with either electron-donating groups (**2a**, **2b**) or withdrawing groups (**2d**, **2e**). As shown in Table 1, we observed the longest emission wavelength in the case of electron-deficient trifluoromethyl-containing **2e** with additional 100-nm red shift from **2c**. Electron-withdrawing cyano moiety at the R_2 position also caused 80-nm red shift from **2b** to **2d**. To further extend the π-conjugation system, we synthesized **3a–i** as Class III by introducing various aryl moieties at the R_1 position. As expected, the phenyl-containing **3e** has 50-nm longer emission wavelength than methyl-containing **2c**. It is worth mentioning that the electron poorness in aryl moieties at the R_1 position can make more efficient push-pull interaction with the dimethylamino group, which led to gradual red shifts of emission

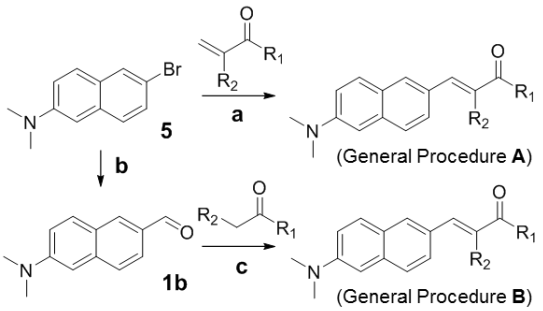

Scheme 1. General synthetic schemes for designed naphthalene-based fluorophores; Desired molecules were synthesized through general procedure **A** (**2a** and **2b**) or **B** (**2c–e, 3a–i,** and **4a–f**) depending on their substituents. Reaction conditions: a) $NaHCO_3$, $Pd(PPh_3)_2Cl_2$, DMF, 140 °C, 8 h; b) n-BuLi, DMF, THF, −78 °C→0 °C, 3 h; c) NaOH, ethanol, water, r.t., 24 h or acetic acid, piperidine, ethanol, reflux, 8 h.

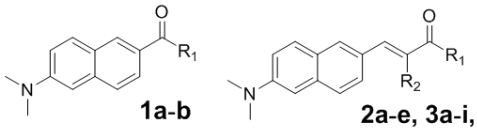

Cpd.	R_1	R_2	λ_{ex} [a]	λ_{em}	δΦ	λ_{ex} [b]	ε	Φ	εΦ
1a	CH_3		740	455	22	354	47k	0.62	29k
1b	H		750	463	30	373	31k	0.84	26k
2a	$N(CH_3)_2$	H	740	485	79	361	25k	1.00	25k
2b	OCH_3	H	760	507	74	382	52k	0.96	50k
2c	CH_3	H	750	536	92	388	60k	0.93	56k
2d	OCH_3	CN	840	591	7.5	455	16k	0.15	2.4k
2e	CF_3	H	900	632	1.2	461	33k	0.04	1.3k
3a	4-NH_2Ph	H	820	565	74[c]	414	63k	0.40	25k
3b	3,4-$(CH_3O)_2$Ph	H	840	584	111	422	50k	0.57	29k
3c	4-CH_3OPh	H	840	586	88	423	37k	0.51	19k
3d	4-CH_3Ph	H	840	590	100	420	29k	0.49	14k
3e	Ph	H	840	599	71	423	37k	0.46	17k
3f	4-FPh	H	840	602	74	423	35k	0.46	16k
3g	4-CF_3Ph	H	900	650	1.0	436	17k	0.05	0.9k
3h	4-CH_3COPh	H	940	657	0.3	444	33k	0.006	0.2k
3i	4-CNPh	H	940	667	0.3	449	25k	0.012	0.3k
4a	pyrrol-2-yl	H	820	567	98	412	24k	0.59	16k
4b	furan-2-yl	H	840	601	89	427	20k	0.61	12k
4c	thiophen-2-yl	H	860	612	52	431	40k	0.38	17k
4d	pyrid-3-yl	H	840	625	18	435	36k	0.18	7.9k
4e	pyrid-2-yl	H	840	633	6.1	437	34k	0.08	2.4k
4f	pyrid-4-yl	H	840	646	0.9	441	52k	0.03	0.5k

Table 1. Two-photon and one-photon photophysical properties of **1a–b**, **2a–e**, **3a–i**, **4a–f** in DMF; λ_{ex} = fluorescence excitation wavelength (nm); λ_{em} = emission wavelength (nm); δΦ = two-photon cross section (GM, 10^{-50} $cm^4 \cdot s \cdot photon^{-1}$); ε = molar extinction coefficient ($L \cdot mol^{-1} \cdot cm^{-1}$); Φ = absolute quantum yield. [a]Two-photon excitation; [b]One-photon excitation; [c]Local maximum point of two-photon emission fluorescence. The global maximum cross section of **3a** is 129 GM by two-photon excitation at 750 nm.

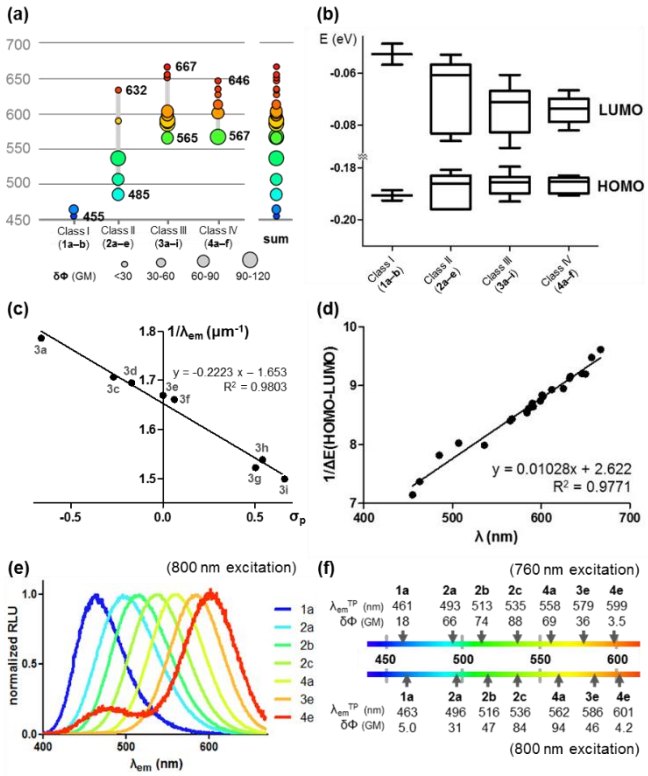

***Figure* 2.** Correlation between predicted and observed photophyscial property data of all 22 prepared fluorescent compounds. a) Two-photon cross section (δΦ) and emission wavelength of **1a–b**, **2a–e**, **3a–i**, **4a–f**; size of circle represents two-photon cross section; y-value and color of circle represent the emission wavelength. b) HOMO and LUMO energy levels of **1a–b**, **2a–e**, **3a–i**, **4a–f** were plotted in vertical box plot. c) Tendency between Hammett constant (σ_p) and emission wavelength of **3a–i** as the substituent changes. d) Linear regression between emission wavelength (nm) and inverse of HOMO–LUMO energy gap (1/eV). e) Normalized fluorescence intensity of **1a**, **2a**, **2b**, **2c**, **4a**, **3e**, and **4e** originated from double excitation with 800 nm. f) Emission wavelength (nm) and cross sections (δΦ) of two-photon fluorescence of **1a**, **2a**, **2b**, **2c**, **4a**, **3e**, **4e**, and **3i** excited by 760 or 800 nm, respectively.

wavelength from 565 nm (**3a** with 4-amino-phenyl group) to 667 nm (**3i** with 4-cyanophenyl group), which is consistent with our *in silico* prediction of emission wavelength on the basis of HOMO–LUMO energy gap. Finally, Class IV consists of **4a–f** through the substitution of aryl moieties in **3e** with heteroaromatic ring systems. Depending on the electron richness in heteroaromatic rings at the R_1 position, we successfully generated fluorophores with 567 nm (**4a**) to 646 nm (**4f**) of emission wavelength; bathochromic shift of fluorescence was occurred systematically as the R_1 substituents were changed from pyrrol-2-yl (**4a**), furan-2-yl (**4b**), and to thiophen-2-yl (**4c**), or from pyrid-3-yl (**4d**), pyrid-2-yl (**4e**), and to pyrid-4-yl (**4f**), respectively (Table 1). This trend of bathochromic shift in Class IV is highly correlated with electronic nature of heteroaromatic rings (Figure S2).

Fluorescent emission wavelength of these fluorophores effectively covers full visible-color range and their brightness is comparable or better than original acedan **1a** with two-photon (δΦ) excitation (Table 1 and size of circle in Figure 2a) as well as one-photon (εΦ) excitation (Figure S3). Although it was predicted, it is disappointing to observe that the fluorescence quantum yield was decreased upon the increase of emission wavelength in our naphthalene-based fluorophores with λ_{em} greater than 600 nm. The observed emission wavelength in each class of fluorophores was well-matched with the calculated energy gap between HOMO and LUMO (Table S1). In fact, electronic character of acetyl group in **1a** was significantly altered by the elongation of π-conjugated system via an insertion of olefin unit or the further attachment of aromatic ring, which lowers energy levels of LUMO in Class II (**2a–e**), III (**3a–i**), and IV (**4a–f**), compared to **1a** (Figure 2b). The systematic alteration of electronic deficiency in aromatic rings in Class III, quantified by Hammett constant (σ_p), showed the linear correlation with the inverse of fluorescence emission wavelength (Figure 2c and S4). In addition, the observed emission wavelength of each fluorophore showed an excellent linear correlation with the inverse of HOMO–LUMO energy gap (Figure 2d), which confirmed the predictability of emission wavelength in our two-photon fluorophores. Moreover, there is a possibility for two-photon multicolor fluorescence imaging with our fluorophores in a visible light range when we apply appropriate light source. With double excitation with the IR-range laser source at 800 nm, we simultaneously observed blue-to-red two-photon fluorescence (Figure 2e). It is worth mentioning that our representative fluorophores **1a**, **2a**, **2b**, **2c**, **4a**, **3e**, and **4e** showed their unique two-photon cross sections upon double excitation at 760 and 800 nm, respectively (Figure 2f). This unique feature of a full visible-color coverage of two-photon fluorescence with double excitation at a single fixed wavelength can be an essential element for the further application into multiplexed full-color bioimaging.

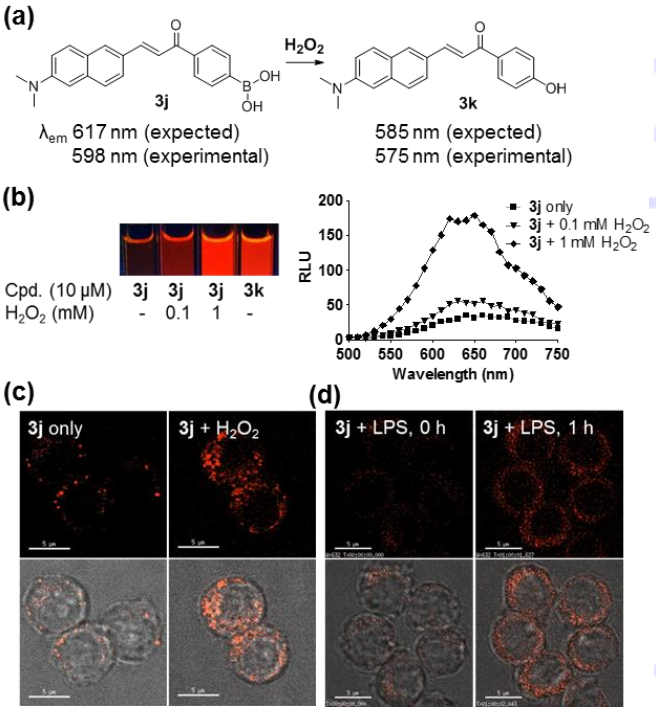

Figure 3. Design strategy and biological application of H_2O_2 fluorescent sensor. a) H_2O_2 sensor **3j** was prepared in a single step from **5**. Emission wavelengths of **3j** and **3k** were well matched with observed data within a 20 nm deviation range; b) **3j** was transformed to **3k** upon *in vitro* treatment of exogenous H_2O_2. (11-fold increase at 641 nm, full conversion was checked by LC-MS). c) Fluorescence images of **3j** in Raw 264.7 cells upon treatment of exogenous H_2O_2. After 20-min treatment with 2 μM **3j**, Raw 264.7 cells were incubated in the presence (right) or absence (left) of 200 μM H_2O_2 for 1 h. d) Raw 264.7 cells were pretreated with 1 μM **3j** for 20 min, and then time-lapse images were taken upon addition of LPS (500 ng/mL). Fluorescence Images (red) were taken from λ_{ex} 438 nm/λ_{em} 632 nm. Scale bar is 5 μm.

For the application of our emission-tunable two-photon fluorophores, we designed and synthesized a fluorogenic H_2O_2 sensor **3j** by one-step reaction using intermediate **5**. As shown in Figure 3a, **3j** and H_2O_2-reacted product **3k** are categorized in Class III because they contain substituted phenyl moieties at the R_1 position. Furthermore, their properties are suitable for the rational design of red-shifted two-photon sensors. Based on the calculated HOMO–LUMO energy gap of **3j** and **3k**, the predicted emission wavelengths using linearity in Figure 2d were within a 20-nm range of deviation from the observed emission wavelength, 598 nm and 575 nm, respectively. When we measured the brightness of one-photon (εΦ: 8100, 15000 $L \cdot mol^{-1} \cdot cm^{-1}$) and two-photon (δΦ: 13, 71 GM) excited fluorescence of **3j** and **3k** at their emission maxima (Figure S5), respectively, we envisioned that the functional group transformation by oxidative stress from borono (**3j**) to hydroxyl group (**3k**) in our naphthalene-based fluorophore can make novel fluorogenic sensor for hydrogen peroxide, an endogenous reactive oxygen species (Figure 3a). To test our hypothesis, **3j** was treated with H_2O_2 in test tubes, which converts **3j** to **3k** in a dose- and time-dependent manner (Figure S6). As shown in Figure 3b, we observed 11-fold increase of fluorescence intensity at 641 nm upon treatment with hydrogen peroxide. Then, we examined whether fluorogenic H_2O_2 sensor **3j** is applicable in living cells. After pre-incubation with **3j**, Raw 264.7 macrophage cells were treated with H_2O_2 or vehicle, which led to the increase of fluorescence intensity in cytoplasm (Figure 3c). Once we confirmed the fluorogenic characteristics of **3j** toward exogenous H_2O_2 in the cellular system, we further tested whether the endogenous H_2O_2 could be detected by **3j**. Raw 264.7 cells were incubated with **3j** followed by the treatment with lipopolysaccharide (LPS), which stimulates the immune response in macrophage cells and triggers the release of various toxic chemokines, including hydrogen peroxide and nitric oxide. As shown in Figure 3d, the LPS-treated cells showed a gradual increase of fluorescence intensity in cytosol while vehicle-treated cells did not.

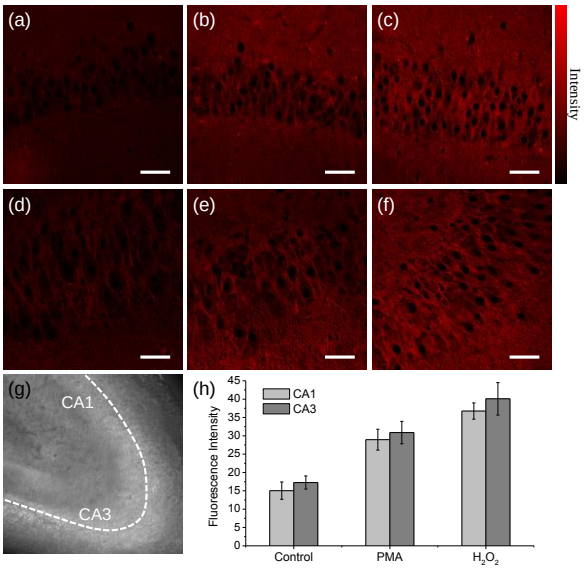

Figure 4. TPM images of a rat hippocampal slice stained with (a, d) 5 μM **3j**. A rat hippocampal slices were pretreated with (b, e) PMA (5 μg mL^{-1}) for 30 min and (c, f) 1 mM H_2O_2 for 30 min before labeling with 5 μM **3j**. (a–c) CA1 and (d–f) CA3 regions. (g) Bright-field image of the CA1 and CA3 regions at 10x magnification. (h) Average TPEF intensities in (a–f). The TPEF were collected at 550–700 nm upon excitation at 820 nm with fs pulse. Scale bars: (a–f) 48 μm.

Finally, we investigated the utility of **3j** for tissue imaging applications by using two-photon microscopy (TPM). Two-photon excited fluorescence facilitates to visualize organs *ex vivo* due to the lengthened penetration depth. Therefore, we applied this H_2O_2 sensor into the two-photon *ex vivo* imaging. A fresh rat hippocampal slice was incubated with **3j** and the TPM images were collected upon excitation with 820 nm with femtosecond pulses. The images displayed weak two-photon excited fluorescence (TPEF) intensities in the CA1 and CA3 regions (Figure 4a and 4d). The TPEF intensities in both regions increased after treatment with H_2O_2 (Figure 4c, 4f, and 4h). Similar result was observed when the tissue was stimulated with phorbol-12-myristate-13-acetate (PMA), which induces cellular H_2O_2 generation through inflammation processes (Figure 4b and 4e). Hence, our probe reports the increase of endogeneous H_2O_2 in living tissue. The successful application of hydrogen peroxide sensor **3j** in the cellular imaging by one-photon excitation as well as *ex vivo* imaging by two-photon excitation clearly confirmed that our naphthalene-based fluorophore can be utilized for the rational development of simple and predictable fluorescence sensors.

In summary, we systematically constructed 22 naphthalene-based two-photon fluorophores with a full coverage of visible light emission. Based on ICT-based structural motif in **1a**, the emission wavelength of our fluorophores can be predicted with high accuracy due to its linear correlation with the inverse of HOMO–LUMO energy gap. The structure–photophysical property relationship study of our two-photon fluorophore guided the rational development of fluorogenic H_2O_2 sensor **3j**, which exhibits the turn-on fluorescence upon exposure to LPS-mediated endogenous H_2O_2 as well as exogenous H_2O_2 in Raw 264.7 macrophage. Finally, **3j** was effectively applied to two-photon *ex vivo* imaging in a rat hippocampal slice, which was resulted in the visualization of endogenous H_2O_2 with red-colored two-photon fluorescence signal.

Acknowledgements

This work was supported by the Creative Research Initiative Grant (2014R1A3A2030423) and Bio & Medical Technology Development Program (2012M3A9C4048780) funded by the National Research Foundation of Korea (NRF). J.Y.K., Y.-H.S. and D.K. are grateful for the BK21 plus scholarship.

Keywords: two-photon fluorescence • acedan • full visible-color coverage • hydrogen peroxide • turn-on biosensor

[1] a) J. V. Frangioni, *Curr. Opin. Chem. Biol.* **2003**, *7*, 626–634; b) K. Licha, C. Olbrich, *Adv. Drug Delivery Rev.* **2005**, *57*, 1087–1108; c) V. Ntziachristos, *Annu. Rev. Biomed. Eng.* **2006**, *8*, 1–33; d) J. R. Lakowicz, Principles of Fluorescence Spectroscopy, 3rd ed., Springer-Verlag, New York, 2006.

[2] a) W. R. Zipfel, R. M. Williams,W. W. Webb, *Nat. Biotech.* **2003**, *21*, 1369–1377; b) F. Helmchen, W. Denk, *Nat. Methods* **2005**, *2*, 932–940; c) M. Oheim, D. J. Michael, M. Geisbauer, D. Madsen, R. H. Chow, *Adv. Drug Delivery Rev.* **2006**, *58*, 788–808; d) M. Rumi, J. W. Perry, *Adv. Opt. Photonics* **2010**, *2*, 451–518.

[3] a) H. M. Kim, B. R. Cho, *Chem. Commun.* **2009**, 153–164; b) H. M. Kim, B. R. Cho, *Acc. Chem. Res.* **2009**, *42*, 863–872; (c) H. M. Kim, B. R. Cho, *Chem. Rev.* **2015**, *115*, 5014–5055.

[4] S. Singha, D. Kim, B. Roy, S. Sambasivan, H. Moon, A. S. Rao, J. Y. Kim, T. Joo, J. W. Park, Y. M. Rhee, T. Wang, K. H. Kim, Y. H. Shin, J. Jung, K. H. Ahn, *Chem. Sci.* **2015**, *6*, 4335–4342.

[5] a) M. K. Kim, C. S. Lim, J. T. Hong, J. H. Han, H.-Y. Jang, H. M. Kim, B. R. Cho, *Angew. Chem. Int. Ed.* **2010**, *49*, 364–367; b) H. J. Kim, J. H. Han, M. K. Kim, C. S. Lim, H. M. Kim, B. R. Cho, *Angew. Chem. Int. Ed.* **2010**, *49*, 6786–6789; c) P. S. Mohan, C. S. Lim, Y. S. Tian, W. Y. Roh, J. H. Lee, B. R. Cho, *Chem. Commun.* **2009**, 5365–5367.

[6] H. M. Kim, M. J. An, J. H. Hong, B. H. Jeong, O. Kwon, J.-Y. Hyon, S.-C. Hong, K. J. Lee, B. R. Cho, *Angew. Chem. Int. Ed.* **2008**, *47*, 2231–2234.

[7] C. Chung, D. Srikun, C. S. Lim, C. J. Chang, B. R. Cho, *Chem. Commun.*, **2011**, *47*, 9618–9620.

[8] a) J. H. Lee, C. S. Lim, Y. S. Tian, J. H. Han, B. R. Cho, *J. Am. Chem. Soc.* **2010**, *132*, 1216–1217; b) H. M. Kim, B. H. Jeong, J.-Y. Hyon, M. J. An, M. S. Seo, J. H. Hong, K. J. Lee, C. H. Kim, T. Joo, S.-C. Hong, B. R. Cho, *J. Am. Chem. Soc.* **2008**, *130*, 4246–4247; c) B. E. Cohen, T. B. McAnaney, E. S. Park, Y. N. Jan, S. G. Boxer, L. Y. Jan, *Science* **2002**, *296*, 1700–1703.

[9] A. P. Silva, H. Q. N. Gunaratne, T. Gunnlaugsson, A. J. M. Huxley, C. P. McCoy, J. T. Rademacher, T. E. Rice, *Chem. Rev.* **1997**, *97*, 1515–1566.

[10] a) P. D. Zoon, I. H. M. van Stokkum, M. Parent, O. Mongin, M. Blanchard-Desce, A. M. Brouwer, *Phys. Chem. Chem. Phys.* **2010**, *12*, 2706–2715; b) E. Kim, M. Koh, J. Ryu, S. B. Park, *J. Am. Chem. Soc.* **2008**, *130*, 12206–12207; c) E. Kim, M. Koh, B. J. Lim, S. B. Park, *J. Am. Chem. Soc.* **2011**, *133*, 6642–6649.

[11] a) N. A. Murugan, J. Kongsted, H. Ågren, *J. Chem. Theory Comput.* **2013**, *9*, 3660–3669; b) E. Kim, Y. Lee, S. Lee, S. B. Park, *Acc. Chem. Res.* **2015**, *48*, 538–547.

[12] a) R. C. Hilborn, *Am. J. Phys.* **1982**, *50*, 982–986; (b) Y. Lee, A. Jo, S. B. Park, *Angew. Chem. Int. Ed.* **2015**, *54*, 15689–15693.

[13] A. S. Rao, D. Kim, T. Wang, K. H. Kim, S. Hwang, K. H. Ahn, *Org. Lett.* **2012**, *14*, 2598–2601.

Entry for the Table of Contents (Please choose one layout)

COMMUNICATION

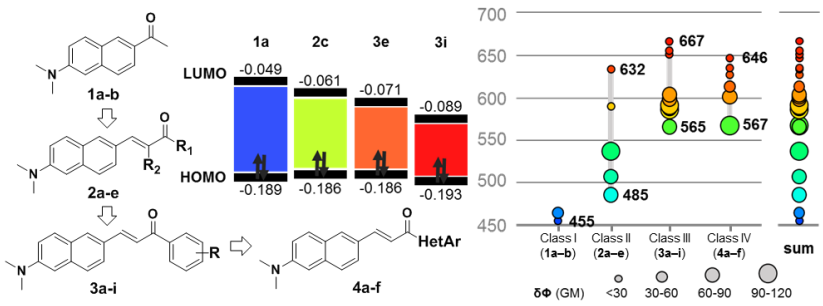

*Ja Young Koo, Cheol Ho Heo, Young-Hee Shin, Dahahm Kim, Chang Su Lim, Bong Rae Cho, Hwan Myung Kim, and Seung Bum Park**

Page No. – Page No.

Readily Accessible and Predictable Naphthalene-based Two-photon Fluorophore with Full Visible-color Coverage

Herein we reported 22 naphthalene-based two-photon fluorophores with synthetic feasibility and a full coverage of visible color emission wavelengths, which were well predicted by *in silico* analysis. Our two-photon fluorophore allows the visualization of multicolor images by two-photon excitation with single wavelength and the rational design of a turn-on two-photon fluorescence sensor for endogenous H_2O_2 in Raw 264.7 macrophage and rat brain hippocampus *ex vivo*.